◆ Human Brain Mapping 34:3376–3391 (2013) ◆

Diffusion Tensor Imaging Based Network Analysis Detects Alterations of Neuroconnectivity in Patients with Clinically Early Relapsing-Remitting Multiple Sclerosis

Yang Li,[1] Valerie Jewells,[2] Minjeong Kim,[1] Yasheng Chen,[1] Andrew Moon,[3] Diane Armao,[3,4] Luigi Troiani,[5] Silva Markovic-Plese,[4] Weili Lin,[1] and Dinggang Shen[1]*

[1]*Biomedical Research Imaging Center (BRIC), Department of Radiology, University of North Carolina at Chapel Hill, North Carolina*
[2]*Division of Neuroradiology, Department of Radiology, University of North Carolina at Chapel Hill, North Carolina*
[3]*Department of Radiology, University of North Carolina at Chapel Hill, North Carolina*
[4]*Department of Pathology and Laboratory Medicine, University of North Carolina at Chapel Hill, North Carolina*
[5]*Department of Neurology, University of North Carolina at Chapel Hill, North Carolina*

Abstract: Although it is inarguable that conventional MRI (cMRI) has greatly contributed to the diagnosis and assessment of multiple sclerosis (MS), cMRI does not show close correlation with clinical findings or pathologic features, and is unable to predict prognosis or stratify disease severity. To this end, diffusion tensor imaging (DTI) with tractography and neuroconnectivity analysis may assist disease assessment in MS. We, therefore, attempted this pilot study for initial assessment of early relapsing-remitting MS (RRMS). Neuroconnectivity analysis was used for evaluation of 24 early RRMS patients within 2 years of presentation, and compared to the network measures of a group of 30 age-and-gender-matched normal control subjects. To account for the situation that the connections between two adjacent regions may be disrupted by an MS lesion, a new metric, network communicability, was adopted to measure both direct and indirect connections. For each anatomical area, the brain network communicability and average path length were computed and compared to characterize the network changes in efficiencies. Statistically significant ($P < 0.05$) loss of communicability was revealed in our RRMS cohort, particularly in the frontal and hippocampal/parahippocampal regions as well as the motor strip and occipital lobes. Correlation with the 25-foot Walk test with communicability measures in the left superior frontal ($r = -0.71$) as well as the left superior temporal gyrus ($r = -0.43$) and left postcentral gyrus ($r = -0.41$) were identified. Additionally identified were increased communicability between the deep gray matter structures (left thalamus and putamen) with the major interhemispheric and intrahemispheric white matter tracts, the corpus callosum, and cingulum, respectively. These foci

Yang Li and Valerie Jewells contributed equally to this work.

Contract grant sponsor: Supported in part by NIH; Contract grant numbers: EB006733, EB008374, EB009634, MH088520, AG041721.

*Correspondence to: Dinggang Shen, Department of Radiology and BRIC, University of North Carolina at Chapel Hill, 130 Mason Farm Road, Chapel Hill, NC 27599-7513, USA.
E-mail: dgshen@med.unc.edu

Received for publication 29 November 2011; Revised 1 May 2012; Accepted 29 May 2012
DOI: 10.1002/hbm.22158
Published online 15 September 2012 in Wiley Online Library (wileyonlinelibrary.com).

of increased communicability are thought to represent compensatory changes. The proposed DTI-based neuroconnectivity analysis demonstrated quantifiable, structurally relevant alterations of fiber tract connections in early RRMS and paves the way for longitudinal studies in larger patient groups. *Hum Brain Mapp 34:3376–3391, 2013.*

Key words: diffusion tensor imaging; multiple sclerosis; network analysis; indirect connections

INTRODUCTION

While less prominent than demyelination, the loss of axons in multiple sclerosis (MS) was described as early as 1868 by Charcot [Charcot, 1868]. Over recent years, axonal loss has spawned interest as the critical component of progressive disease and permanent neurologic deficit [Compston et al., 2006]. Axonal injury and transection are characteristic of both early and chronic MS lesions [Trapp et al., 1998]. Diffusion tensor imaging (DTI) has become a useful tool in defining parameters of demyelination and axonal loss [Gong et al., 2009; Mottershead et al., 2003; Schmierer et al., 2007; Skudlarski et al., 2008]. A formidable challenge to the application of MR imaging in MS exists in tracking the course of the disease in an effort to elucidate mechanisms causing the accumulation of irreversible disability.

The application of functional MRI (fMRI) to the assessment of central nervous system function in MS patients has shown the presence and efficacy of brain adaptive mechanisms which may contribute, in some phases of the disease, to limiting clinical consequences of disease-related injury [Rocca et al., 2005]. Failure of these adaptive mechanisms may prove to be among the major factors responsible for the accumulation of irreversible injury [Filippi and Rocca, 2009]. In addition, the development of sophisticated, postprocessing methods has permitted the structural analysis of brain connectivity in normal and diseased patients [He et al., 2009]. Advances in DTI and tractography have spurred the development of brain neuroconnectivity techniques, which define and quantify anatomical links between remote brain regions by axonal fiber pathways [Guye et al., 2010]. Recent research using diffusion tensor tractography has revealed reduced network efficiency in the white matter structural networks in MS patients [Shu et al., 2011].

Combining different, noninvasive, and in vivo modalities with these new analytical strategies is a promising way to increase the understanding of adaptive mechanisms occurring over the course of the accumulation of disability [Zhang et al., 2011]. Such quantifiable alterations in brain connectivity may already be in evidence in newly diagnosed patients with relapsing-remitting MS (RRMS). To test this hypothesis, we performed DTI with neuroconnectivity analysis to evaluate clinically early RRMS patients and compared these findings with healthy volunteers. To the best of our knowledge, this study represents, for the first time, the use of combined DTI and neuroconnectivity network analysis and probes the fiber pathway remodeling and alterations in RRMS. In addition, different from the previous network analysis metrics applied in MS [He et al., 2009; Shu et al., 2011], the new network metric [Crofts and Higham, 2009; Estrada and Hatano, 2008] adopted is able to account for both direct and indirect connections and is more specific on evaluating the communication efficiency, which provides communicability measure on either region of interest (ROI)-to-ROI or ROI-wise. This new metric could be more suitable in the context of our study of brain networks in MS patients. As direct connections between two adjacent regions may be disrupted by an MS lesion, the measure of communicability via indirect connections plays a more important role.

MATERIALS AND METHODS

Patients

Twenty-four patients within 2 years of diagnosis as RRMS (ages 26–55 years, median 37) and 30 age-and-gender-matched normal controls (NC) were selected for retrospective analysis from a pre-existent MS patient registry (Table I). All patients had disease duration of 32 ± 9 months when the scan was obtained. The diagnosis of MS was made by the treating physician according to the McDonald criteria and patients were excluded if they had additional diagnoses that could confound MRI interpretation via physical examination and laboratory analysis. All patients had experienced at least two episodes suggestive of MS, and their MRI exams were 1–2 years after RRMS diagnosis. Clinical impairment was assessed with the Timed 25-foot Walk test, a portion of the MS functional composite (MSFC), and the Expanded Disability Status scale (EDSS). The time between clinical examination and imaging was 3–8 days. Not all components of the MSFC were performed in all patients, limiting the available clinical data for comparative analysis. The EDSS combines scores from eight functional scales (assessing a patient's

TABLE I. Characteristics of the participants

	Number	Age (mean ± STD)	Gender (F/M)	Median EDSS
RRMS	24	38.8 ± 9.0	17/7	1.75
Normal control	30	37.8 ± 8.6	21/11	N/A

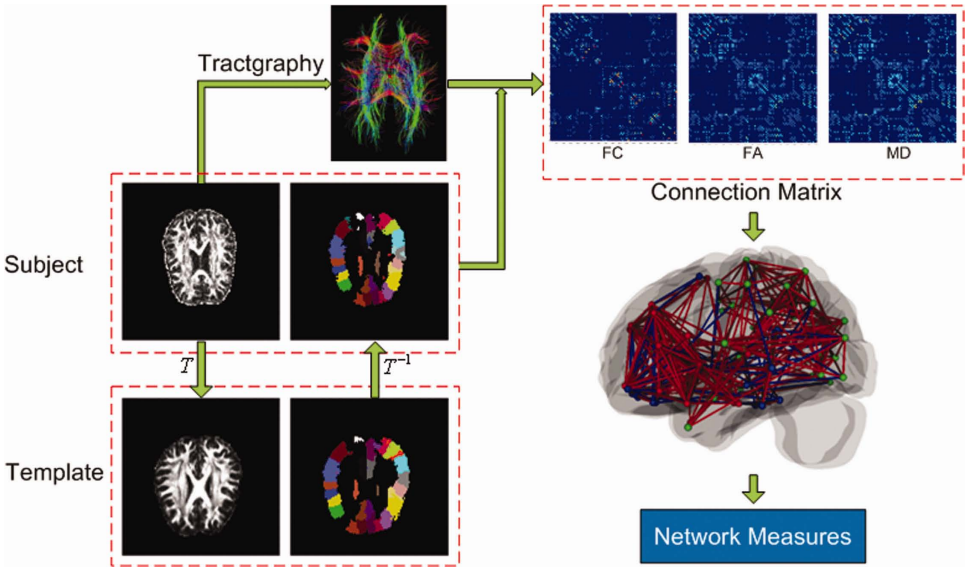

Figure 1.
Flowchart of the network construction. [Color figure can be viewed in the online issue, which is available at wileyonlinelibrary.com.]

ability to ambulate, use their arms, communicate, and swallow) into an 11-point ordinal scale (0 = normal status and 10 = death due to MS). The median EDSS score for the 24 RRMS patients was 1.75 (range 1–4). RRMS patients had been receiving anti-inflammatory therapy for various periods of time when the MRI data were acquired. A written informed consent to participate was obtained from all patients in accordance with the declaration of National Institute of Health (NIH) ethics standards. This is an institutional review board (IRB) approved study.

Data Acquisition

Diffusion scans were obtained on a 3.0T Siemens Allegra head-only scanner with maximum gradient strength of 40 mT m^{-1}. Diffusion-weighted data were acquired using echo planar imaging (TR = 8,500 ms, TE = 80 ms, 2.0-mm thick axial slices, voxel size of 2.0 × 2.0 × 2.0 mm, 5 averages, FOV = 256 × 256 mm, matrix = 128 × 128). The diffusion weighting was isotropically distributed in six directions using a b value of 1,000 s mm^{-2}. About 1-mm isotropic T_1 (MP-RAGE, TE = 4.38 ms, TR = 1,750 ms, flip angle 8°, T_1 = 900 ms, oversampling 10%, FOV = 256 × 256, 1 average, 1 concatenation) and T_2 (TE = 354 ms, TR = 2,500 ms, oversampling 30%, FOV = 256 × 256, 1 average, 1 concatenation) images were also performed. From these conventional MRI sequences, T_1 and T_2 lesion loads were obtained.

Image Preprocessing

Standard preprocessing steps for general brain image analysis were performed to reduce image noise and remove the skull and surrounding soft tissues. To achieve optimal skull stripping, we combined automatic method with manual editing to ensure accurate and complete skull removal. Skull stripping was initially performed on the B = 0 image, and the resultant mask was then applied to the tensor fitting/reconstruction process.

Network Construction

Construction of the DTI Template

Preceding brain network construction, individual subject brain volumes were partitioned into different anatomical regions according to the widely accepted Anatomical Automatic Labeling (AAL) atlas [Tzourio-Mazoyer et al., 2002]. However, as this atlas only has T_1-weighted structural images, the DTI image of each subject cannot be directly registered to the AAL atlas. Hence, a healthy normal subject with coregistered DTI image and corresponding T_1 image was selected as a new template. Then, by registering the T_1 image of the AAL atlas onto the T_1 image of the selected template, ROIs of the AAL atlas were mapped to the template space. Thus, with the mapped ROI labels, a new DTI image template is obtained (as indicated as "template" in Fig. 1), which includes the anatomical partitions of the AAL atlas in the space of the selected normal subject.

Network Construction

For each study subject, the reconstructed diffusion tensor volume was registered to the above-constructed DTI template by using tensor-based elastic registration algorithm [Yap et al., 2010; Wu et al., 2006]. Subsequently, the obtained transformation T was inversed (T^{-1}) and applied

to the atlas to map the anatomical labels onto each subject's space (as shown in Fig. 1). The AAL atlas partitions two cerebral hemispheres into 90 anatomical regions (74 cortical and 16 subcortical). Therefore, by mapping the AAL atlas onto each subject, 90 anatomical regions were consistently labeled for each subject.

Tractography was then performed for each subject to quantify structural connectivity between the 90 identified brain regions. Specifically, the streamline was seeded on white matter with fractional anisotropy (FA) >0.5 and propagated by increment of 2 mm every step. The curvature threshold was set to make sure that the step-by-step change of angle is below 30°. The tracking algorithm stopped if the FA <0.3 for the three consecutive steps. Following tractography, the white matter fibers were represented as streamlines in three-dimensional space. For each pair of regions, if one fiber is originated from one brain region and ends in another brain region, the two regions were considered to be "connected" by this fiber. The count of fibers connecting each pair of regions was then measured and used as the indication of the strength of the connection between these two regions. Similarly, the average FA and average mean diffusitivity (MD) along the fiber bundles connecting two regions were also calculated as two other indications of the connection strength. The main reason of including MD and FA into the study is to investigate the moderate white matter changes that are not serious enough to interrupt fibers. As the fiber-count-based network only captures the "dramatic" network changes, FA- and MD-based networks can provide complementary measures to identify subtle fiber changes. Therefore, such a network construction method resulted in three weighted undirected graphs with 90 nodes for each subject, which can be represented in a connection/adjacency matrix. For simplicity, in the remainder of this paper, we refer to the three constructed networks and corresponding adjacency matrices as N_{FC}, N_{FA}, and N_{MD}, respectively.

Communicability and Average Path Length

Communication between different brain parts can be understood as transmission of information through a network, which is usually considered to take place along geodesic distance. However, in many real-world networks, such as in brain networks with small-worldness feature, the spread of information is not restricted only to the shortest paths. In the context of our study of brain networks in MS patients, connections between two adjacent regions may be disrupted by an MS lesion. However, reorganization of tracts between the regions will still allow communication between the two regions via longer paths bypassing the lesion. Therefore, taking these indirect connections into account would be crucial in this study.

Recently, a new concept of communicability was introduced in [Crofts and Higham, 2009; Estrada and Hatano, 2008] as a quantitative measure of the efficiency with which "information" can spread across a network. This new measure deals with the issue that there is no edge between a pair of nodes, which does not necessarily indicate a low degree of "connectednesses" between two nodes. They define the communicability between two nodes by counting the total number of walks between them, with walks of length k scaled by a factor of $1/k!$, such that the longer walks have less influence than the shorter walks. Compared with other network measures, such as clustering coefficient [Rubinov and Sporns, 2009], the new measure communicability has two main advantages. First, not only the local direct connections but also the long-distance indirect connections are taken into account. Second, more specifically, for each pair of regions, an overall measurement of the connectedness between them can be provided. In a more recent study [Crofts et al., 2010], changes in the contralesional hemisphere following stroke were detected using this measure, but are unseen to the conventional network measures. In this study, we adopted this new measure. A brief introduction of this measure and how it is computed in our study can be found in the Appendix section.

As mentioned above, reorganization of tracts may occur between the regions affected by the lesion, where the reduced direct communicability may be compensated via connections with longer paths. Therefore, it is possible that in some situations, the overall communicability could be maintained. In this case, this type of network change is invisible to the metric communicability. To quantify this, we proposed another network measurement, average path length (APL), which is also defined in the Appendix section.

Statistical Analysis

To determine which brain regions have significant changes in communicability or APL between the two groups, we performed t-tests on the communicability degree ($\deg_{C_i}$) scores for each region. Similarly, to be more specific, for each pair of regions, the communicability C_{ij} and APL_{ij} were also compared between the two groups. Other than the conventional t-test, the network-based statistic (NBS) [Zalesky et al., 2010a] was also used to identify the between-group differences in pairwise communicability C_{ij}. Instead of performing the test individually on each node, the NBS method aims to identify the connected subnetworks in the communicability matrix that significantly differ between groups. Therefore, the NBS has been demonstrated to offer greater statistical power [Verstraete et al., 2011; Zhang et al., 2011] and may reveal more differences that probably have been overlooked with the false discovery rate (FDR) correction, which often uses the conventional t-test.

RESULTS

Group Differences in Communicability Measures

Comparison results for the degree of communicability ($\deg_{C_i}$) between RRMS and NC groups via three adjacency

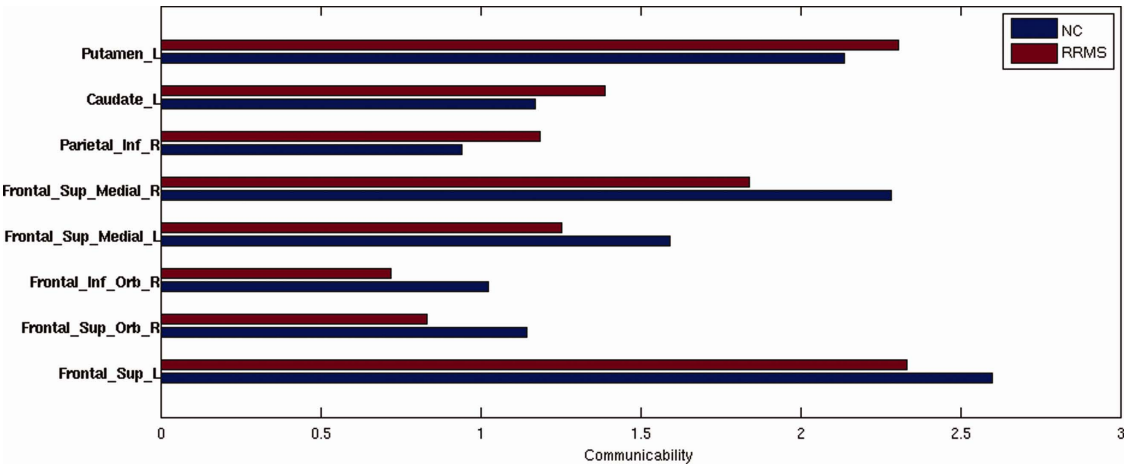

Figure 2.

Comparison of the communicability measure $\deg_{C_i}$ between RRMS and normal control group for the N_{FC} network. Only the regions with significant regional group differences ($P < 0.05$, FDR-corrected) are displayed. [Color figure can be viewed in the online issue, which is available at wileyonlinelibrary.com.]

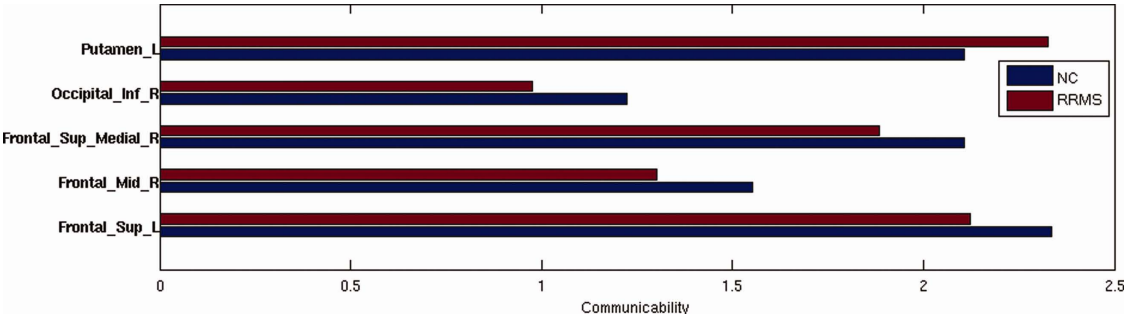

Figure 3.

Comparison of the communicability measure $\deg_{C_i}$ between RRMS and NC group for the N_{FA} network. Only the regions with significant regional group differences ($P < 0.05$, FDR-corrected) are displayed. [Color figure can be viewed in the online issue, which is available at wileyonlinelibrary.com.]

matrices N_{FC} (Fig. 2), N_{FA} (Fig. 3), and N_{MD} (Fig. 4) detect the regions with significant ($P < 0.05$, FDR corrected) connection changes. These parameters consistently reveal reductions in FC, FA, and MD for the connections between different AAL-atlas-defined foci outside of the deep gray matter (GM) (mostly from frontal lobe regions), suggesting loss of axons (FC) and myelin (FA and MD). However, there are multiple tracts revealing increased FC, FA, and MD between deep GM nuclei (putamen and caudate) and other brain regions, as well as increased connections involving the cingulum.

More specifically, comparison results of the pairwise communicability (C_{ij}) between RRMS and NC groups (NBS corrected, $P < 0.05$) are displayed for N_{FC} (Fig. 5), N_{FA} (Fig. 6), and N_{MD} (Fig. 7) as well. These parameters also consistently reveal reductions in FC, FA, and MD for connections between different AAL-atlas-defined foci outside of the deep GM (mostly from frontal lobe regions), and again demonstrate the increased pairwise communicability with increased FC, FA, and MD between the deep GM (putamen and caudate) and cingulum with other brain regions.

Group Differences in APL

The results of APL changes between the two groups are summarized in Table II. As the information travel length is averaged by the unit of information (see Appendix section), Table II shows the 15 region-pairs, between which, to send the same amount of information from one to the other, it travels a significantly longer path in the RRMS group.

The right inferior Orbitofrontal cortex ("Frontal_Inf_Orb_R" in AAL atlas) is one of the regions that are most significantly involved in the APL changes. Correspondingly, in Figure 5, this region also demonstrates significantly decreased communicability between other regions

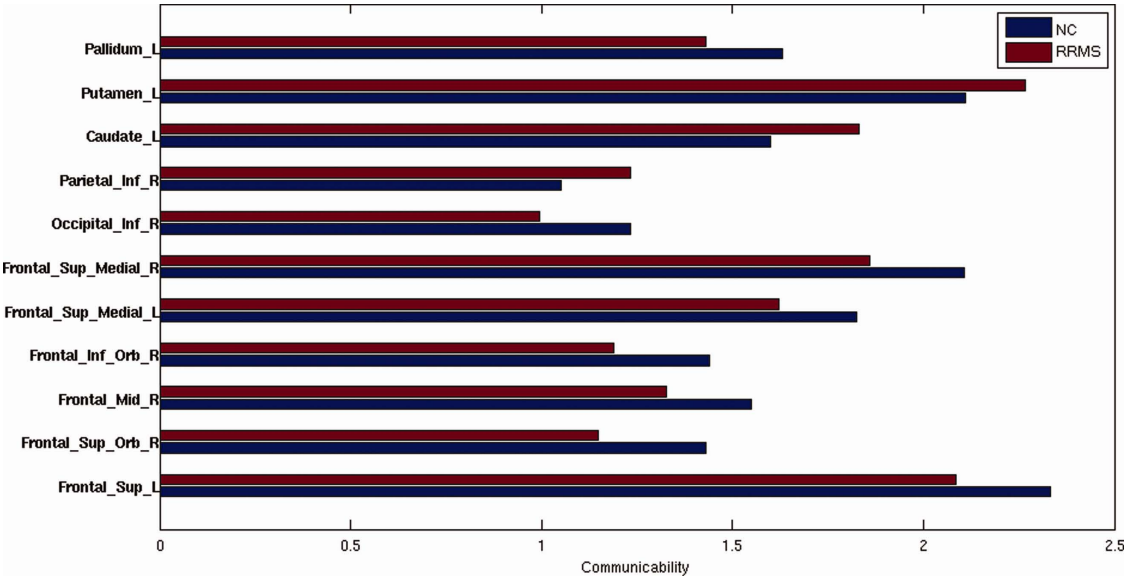

Figure 4.

Comparison of the communicability measure deg_{C_i} between RRMS and NC group for the N_{MD} network. Only the regions with significant regional group differences ($P < 0.05$, FDR-corrected) are displayed. [Color figure can be viewed in the online issue, which is available at wileyonlinelibrary.com.]

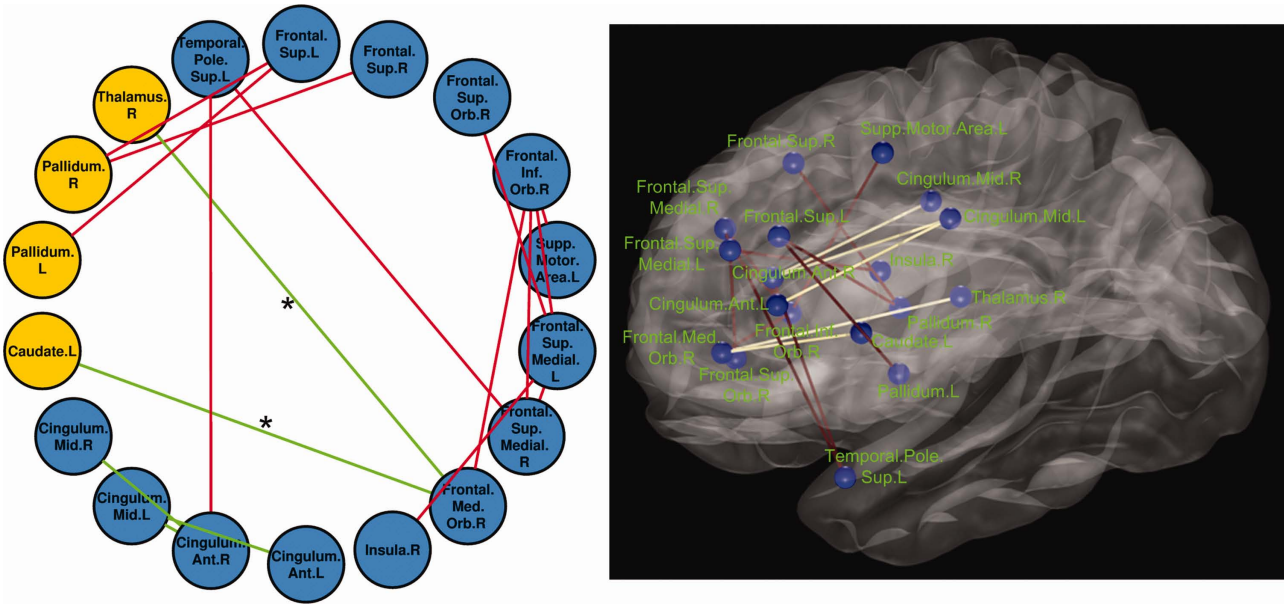

Figure 5.

Comparison of the pairwise communicability C_{ij} between RRMS and NC group for the N_{FC} network. Only region pairs showing a significant difference ($P < 0.05$, by NBS) between the two groups are displayed. Edges with mark "*" indicate $P < 0.05$. Other edges are with $P < 0.001$. The uncorrected P values range between 1e-7 and 1e-5. The left shows the affected regions in a circle layout, in which green and red edges show increased and decreased communicability, respectively. The right indicates the relative positions of these regions in the brain. [Color figure can be viewed in the online issue, which is available at wileyonlinelibrary.com.]

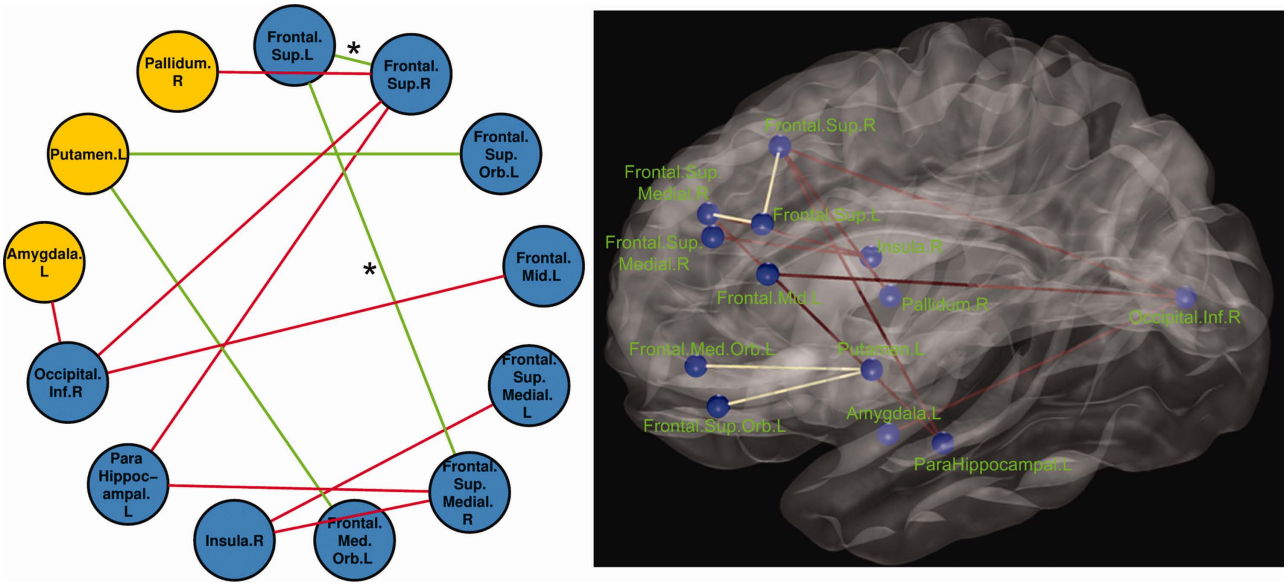

Figure 6.

Comparison of the pairwise communicability C_{ij} between RRMS and NC group for the N_{FA} network. Only region pairs showing a significant difference ($P < 0.05$, by NBS) between the two groups are displayed. Edges with mark "*" indicate $P < 0.05$. Other edges are with $P < 0.001$. The uncorrected P values range between 1e-6 and 1e-5. The left shows the affected regions in a circle-layout, in which green and red edges show increased and decreased communicability, respectively. The right indicates the relative positions of these regions in the brain. [Color figure can be viewed in the online issue, which is available at wileyonlinelibrary.com.]

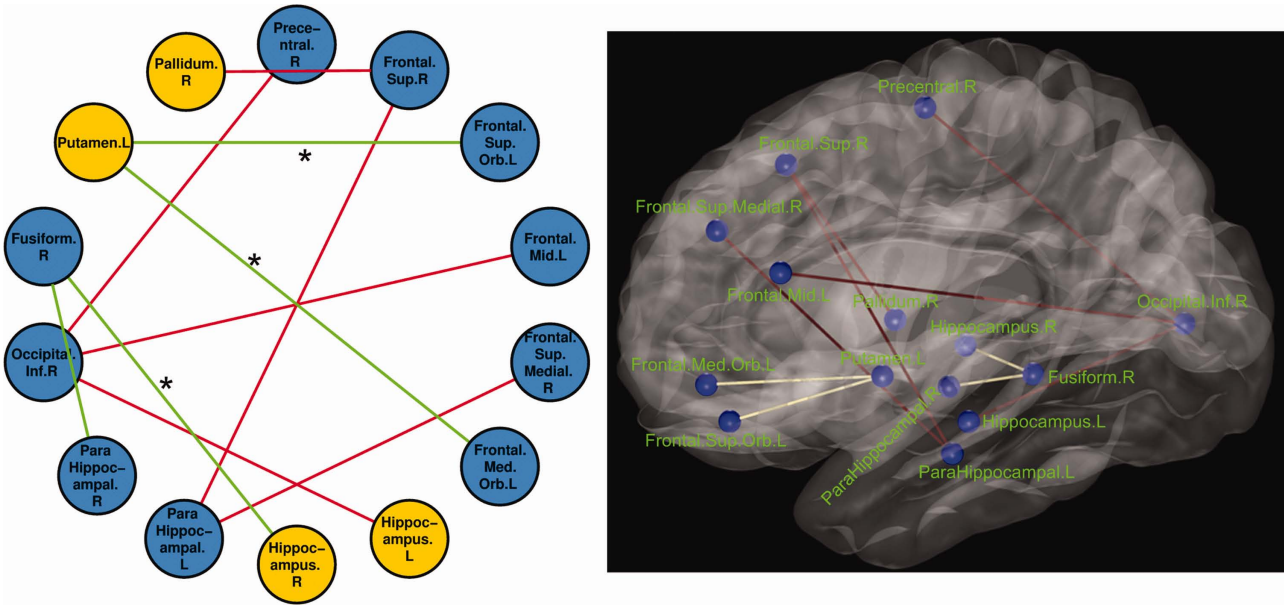

Figure 7.

Comparison of the pairwise communicability C_{ij} between RRMS and NC group for the N_{MD} network. Only region pairs showing a significant difference ($P < 0.05$, by NBS) between the two groups are displayed. Edges with mark "*" indicate $P < 0.05$. Other edges are with $P < 0.001$. The uncorrected P values range between 1e-6 and 1e-5. The left shows the affected regions in a circle-layout, in which green and red edges show increased and decreased communicability, respectively. The right indicates the relative positions of these regions in the brain. [Color figure can be viewed in the online issue, which is available at wileyonlinelibrary.com.]

TABLE II. Region pairs with significant ($P < 0.05$, FDR corrected) APL changes

Region–Region	Increase (+)/ Decreased (−)
Frontal_Inf_Orb_R–Rolandic_Oper_L	+
Frontal_Inf_Orb_R–Frontal_Sup_Medial_L	+
Frontal_Inf_Orb_R–Insula_L	+
Frontal_Inf_Orb_L–Insula_R	+
Frontal_Inf_Orb_R–Hippocampus_L	+
Frontal_Inf_Orb_R–Fusiform_L	+
Frontal_Inf_Orb_R–Temporal_Sup_L	+
Frontal_Inf_Oper_R–Temporal_Pole_Sup_L	+
Frontal_Inf_Tri_R–Temporal_Pole_Sup_L	+
Frontal_Inf_Orb_R–Temporal_Pole_Sup_L	+
Rolandic_Oper_R–Temporal_Pole_Sup_L	+
Frontal_Sup_Medial_R–Temporal_Pole_Sup_L	+
Insula_R–Temporal_Pole_Sup_L	+
Temporal_Pole_Sup_L–Temporal_Pole_Sup_R	+
Frontal_Inf_Orb_R–Temporal_Inf_L	+

"+" denotes the significant increase of APL which was observed in RRMS group, indicating the reduced communication efficiency.

in the RRMS group. These two findings are consistent with each other. A possible explanation is that, although many bypasses were created (and detected by the increased APL) to compensate for the loss of direct/shorter connections, the communicability still cannot be maintained between this region and other brain regions which would have an impact theoretically upon processing speed. It is also not surprising that all the observed APL changes are "increases" which indicates degenerated efficiency of information transformation in the RRMS group.

Probabilistic Lesion Map

Owing to the multifocal and widespread occurrence of MS lesions throughout the brain, alterations of structural neuroconnectivity should be topographically related to the location of focal lesions. To access this relationship, a probabilistic lesion map of the RRMS group was created and is shown in Figure 8. To pictorially illustrate the relationship between lesions and the regions with affected connectivity, the probabilistic lesion map was overlapped with the pair of regions with decreased (Fig. 9) and increased (Fig. 10) communicability. Along the pathway of each region pair with decreased communicability, a high probability of MS lesions is observed. A representative example is shown in Figure 9c, in which the right medial superior frontal cortex ("R_Frontal_Sup_Medial" in AAL) to the left medial superior frontal cortex ("L_Frontal_Sup_Medial" in AAL) connection is through the corpus callosum, in the region of the genu. However, this pathway is compromised by a high concentration of MS lesions, flanking both sides of the genu. Decreased communicability at this site was observed in the RRMS group when compared with NC. In Figure 10, the region pairs with increased communicability are mainly located between deep GM structures, such as the caudate nucleus, and the cortical defined foci. Also identified in this region is the increased communicability between the white matter structures, the anterior, and mid cingulum of both cerebral hemispheres.

Correlation With MSFC Timed 25-foot Walk Test

The communicability metric $\deg_{C_i}$ of each ROI was also correlated to the scores (in seconds) of the MSFC Timed 25-foot Walk test. The regions with the most significant high correlations (either positive or negative) are summarized in Figure 11. The superior frontal gyrus is a structure involved in self-awareness and coordination with actions via the sensory system [Goldberg et al., 2006]. With regard to consistency, the overall communicability of this structure shows high correlation ($r = -0.71$) with the time spent in the 25-foot Walk test. The left superior temporal gyrus ($r = -0.43$) and left postcentral gyrus ($r = -0.41$) also demonstrate decreased communicability that correlated with the results of the 25-foot Walk test. Additionally, the left postcentral gyrus is the location of the primary somatosensory cortex and is the main sensory receptive area for the sense of touch, a required function for the Timed 25-foot Walk test. Other MSFC tests were not performed in the majority of the patients, and therefore were not assessed. Also identified were increased communicability of the left mid cingulum ($r = -0.48$) with two deep GM structures, the left thalamus ($r = -0.41$) and left putamen ($r = -0.43$). We again hypothesize as stated in Group Differences in Communicability Measures section that the increased connections may demonstrate compensation effects. Interestingly, all these regions involve the left hemisphere in our predominantly right-handed participants.

DTI Abnormalities in the Region of the Optic Radiations and Occipital Lobes

Our results also demonstrated multiple areas of neuroconnectivity abnormalities that would have a negative impact upon vision. As stated in Table III, there are neuroconnectivity reductions in the right calcarine cortex, the primary visual cortex for the right visual field of both eyes. Additionally, there are connectivity reductions also in the regions of the right superior occipital, right middle occipital, and left inferior occipital lobes areas of associative and secondary visual cortex. Also identified are bilateral lesions in the regions of the optic radiations (OR) in these patients on the lesion probability map, which may in part explain the loss of axonal fibers in the regions of visual function. Also denoted in Figures 2 and 4, are regions of decreased communicability in the right inferior occipital

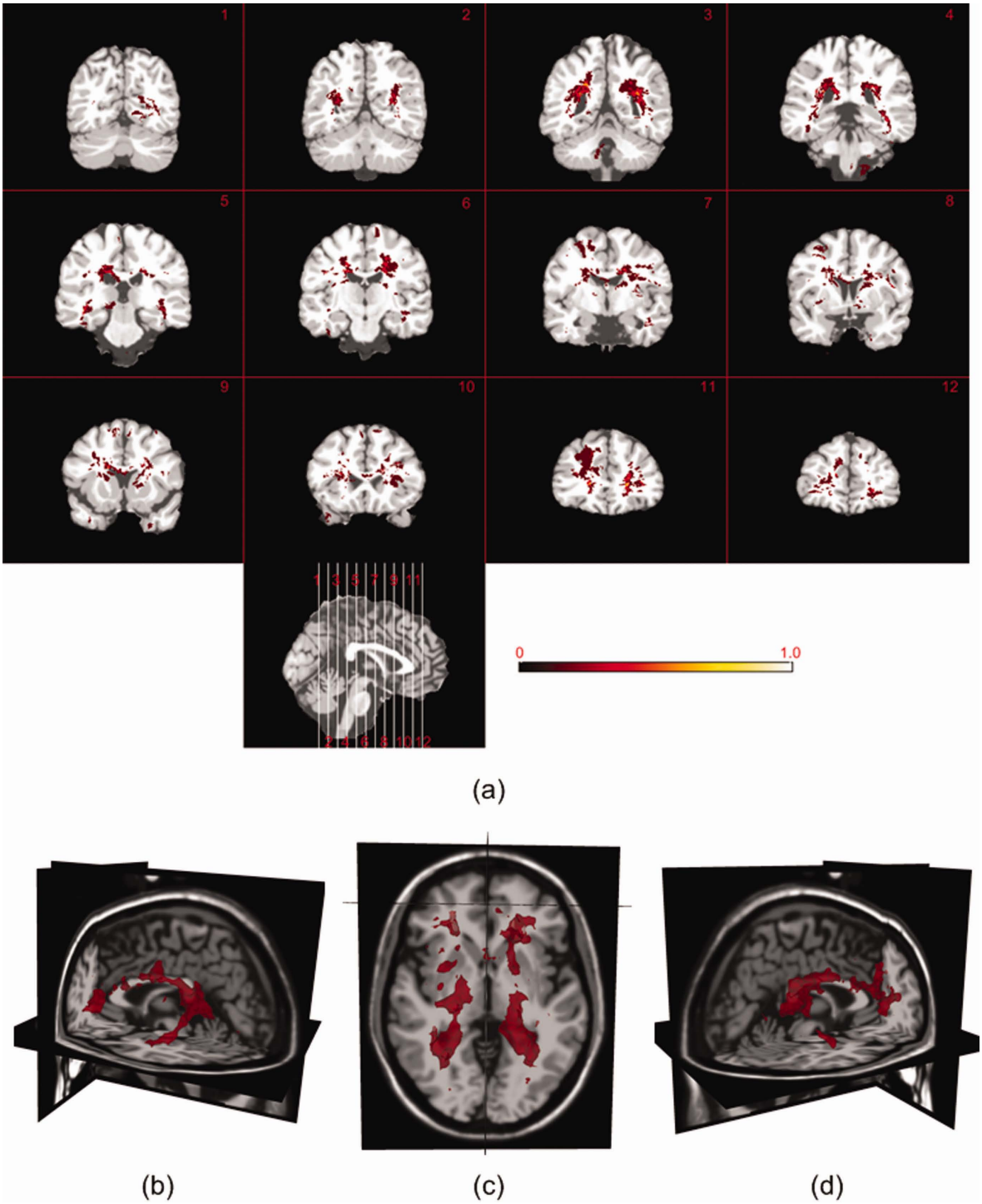

Figure 8.

The probabilistic MS lesion distribution map in two-dimensional (2D) (**a**) and three-dimensional (3D) (**b** and **c**). In 2D map, the color represents the probability of observing a lesion at specific locations in the RRMS group. The 3D map shows the distribution where the probability $P > 0.5$. [Color figure can be viewed in the online issue, which is available at wileyonlinelibrary.com.]

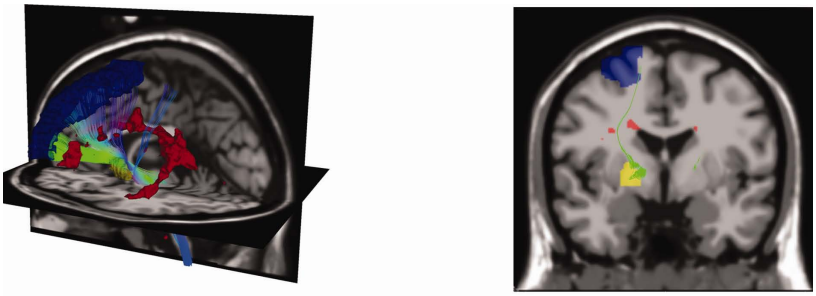

(a) Frontal.Sup.R and Pallidum.R

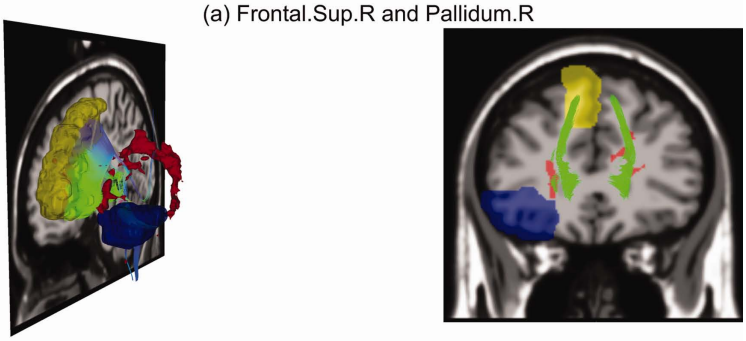

(b) Frontal.Inf.Orb.R and Frontal.Sup.Medial.R

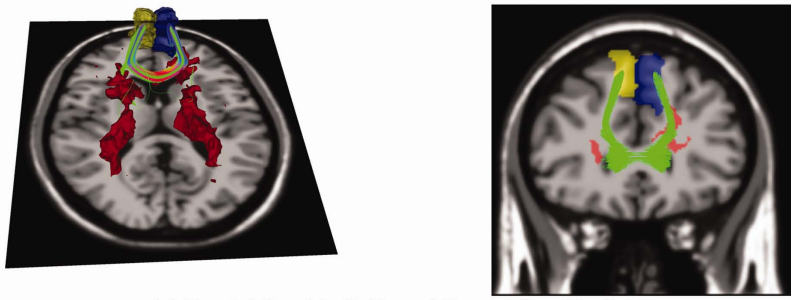

(c) Frontal.Sup.Medial.L and Frontal.Sup.Medial.R

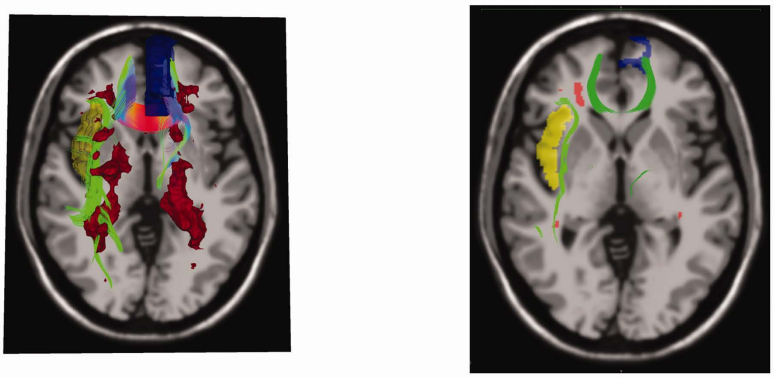

(d) Frontal.Sup.Medial.L and Insula.R

Figure 9.

The pairs of regions with MS-interrupted fiber tracts in between. Some of the pairs with significant degeneration in Figure 5 are displayed here. For each region pair (with blue and yellow foci representing the two regions), a high probability of MS lesions (red) can be observed obstructing the pathway (in one step or between two steps) between the respective regions. In each panel, the left figure shows the regions and fiber tracts in 3D view. To illustrate the relative position more intuitively, the tracts are also projected into a 2D view and shown on the right. [Color figure can be viewed in the online issue, which is available at wileyonlinelibrary.com.]

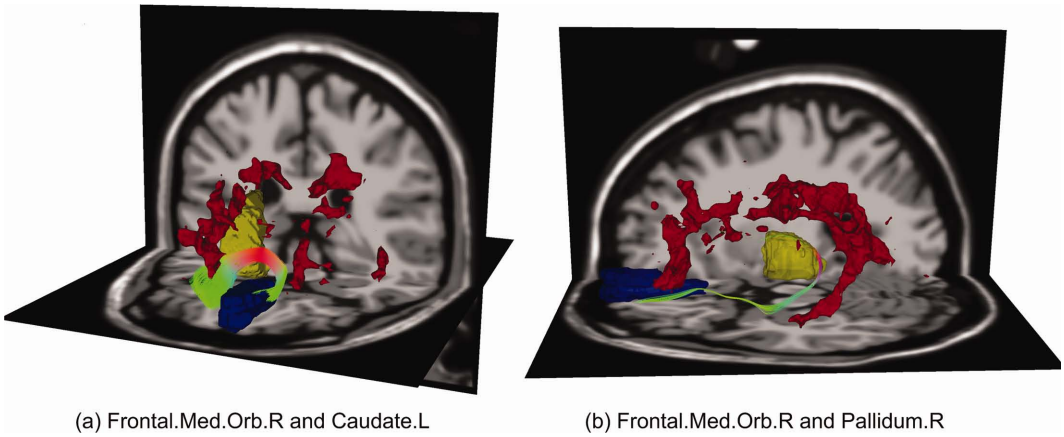

Figure 10.

The locations of the region pairs with increased communicability. Some of the region pairs with significant increase in communicability, as shown in Figure 5, are displayed here. Between each region pair (with blue and yellow foci representing the two regions), there are no MS lesions (red) with high probability observed obstructing the pathway. The observed increased communicability may indicate the compensation effects. [Color figure can be viewed in the online issue, which is available at wileyonlinelibrary.com.]

lobe. A fact that may explain abnormalities in these areas is that nine patients from the 24 RRMS group had a documented history of optic neuritis.

DISCUSSION

In patients with clinically early RRMS, changes in MD, FA, and FC were prominent within frontal and temporal lobes, where the probabilistic lesion map showed an increased proportion of MS plaques. Such abnormalities in DTI parameters in the RRMS group were anticipated due to the sensitivity of MD and FA to general tissue damage and changing patterns of restricted water diffusion associated with alterations in the myelin sheath and axoplasm [Song et al., 2003, 2005]. Moreover, in the present study, significant reductions in FC in the frontal lobes at the level of the anterior corpus callosum (genu) may have distinctive neuroanatomic and neuropathologic correlations. Nerve fiber distribution in the corpus callosum is topographically organized [Aboitiz et al., 1992]. Thin, small caliber fibers are most dense in the genu, representing 72% of the total fiber population in this region [Aboitiz et al., 1992; Hasan et al., 2005]. From a neuropathologic standpoint, an important issue in understanding the mechanisms of axonal injury in MS is the size selective nature of axonal degeneration [Lassmann, 2009]. Small caliber axons are much more vulnerable to injury compared to thick, large caliber axons, creating preferential damage to thin axons [Lassmann, 2009]. Thus, pronounced reductions in communicability and neuroconnectivity between left and right frontal lobes in the region of the genu may be a function of several factors, namely: (1) MS plaques with myelin loss and early axonal injury, (2) secondary Wallerian degeneration, and (3) intrinsic, selective vulnerability of small caliber axons having the highest density within the genu of the corpus callosum (Fig. 8).

An unexpected result in the RRMS cohort was the increase in MD, FA, and FC with increased connectivity in the deep gray nuclei (caudate, putamen, and thalamus) and cingulum, which was not reported in previous works [Filippi et al., 2000; Hasan et al., 2009; Shu et al., 2011]. This new finding may be attributed to the new method, which is more accurate on assessing the influence on indirect brain connections occurring as tracts reroute around lesions. Our results are consistent with quantitative DTI and fMRI reports by other authors. Higher values of MD and FA have been shown in the caudate nucleus, basal ganglia, and thalamus in RRMS patients [Ciccarelli et al., 2001; Hasan et al., 2009; Tovar-Moll et al., 2009]. Increased activation of multiple cortical structures, deep gray nuclei, and cingulum in primary progressive multiple sclerosis (PPMS) patients has been demonstrated with fMRI and DTI tractography [Ceccarelli et al., 2010]. Furthermore, in a large prospective multicenter fMRI international collaborative study, MS patients showed greater brain recruitment of portions of the cingulate gyrus and bilateral caudate and putamen with less hand dexterity [Wegner et al., 2008]. Similar cortical recruitment was also observed in patients with isolated myelitis [Rocca et al., 2006]. Increased thalamic activation using fMRI in RRMS patients has also been identified in patients who recover more quickly from fatigue suggesting a compensatory mechanism [Rocca et al., 2007]. In our study, a significant correlation was found between increased connectivity and communicability of the mid-cingulum, thalamus, and putamen with decreasing performance in the MSFC Timed 25-foot Walk test. Such patterns of fiber tract structural

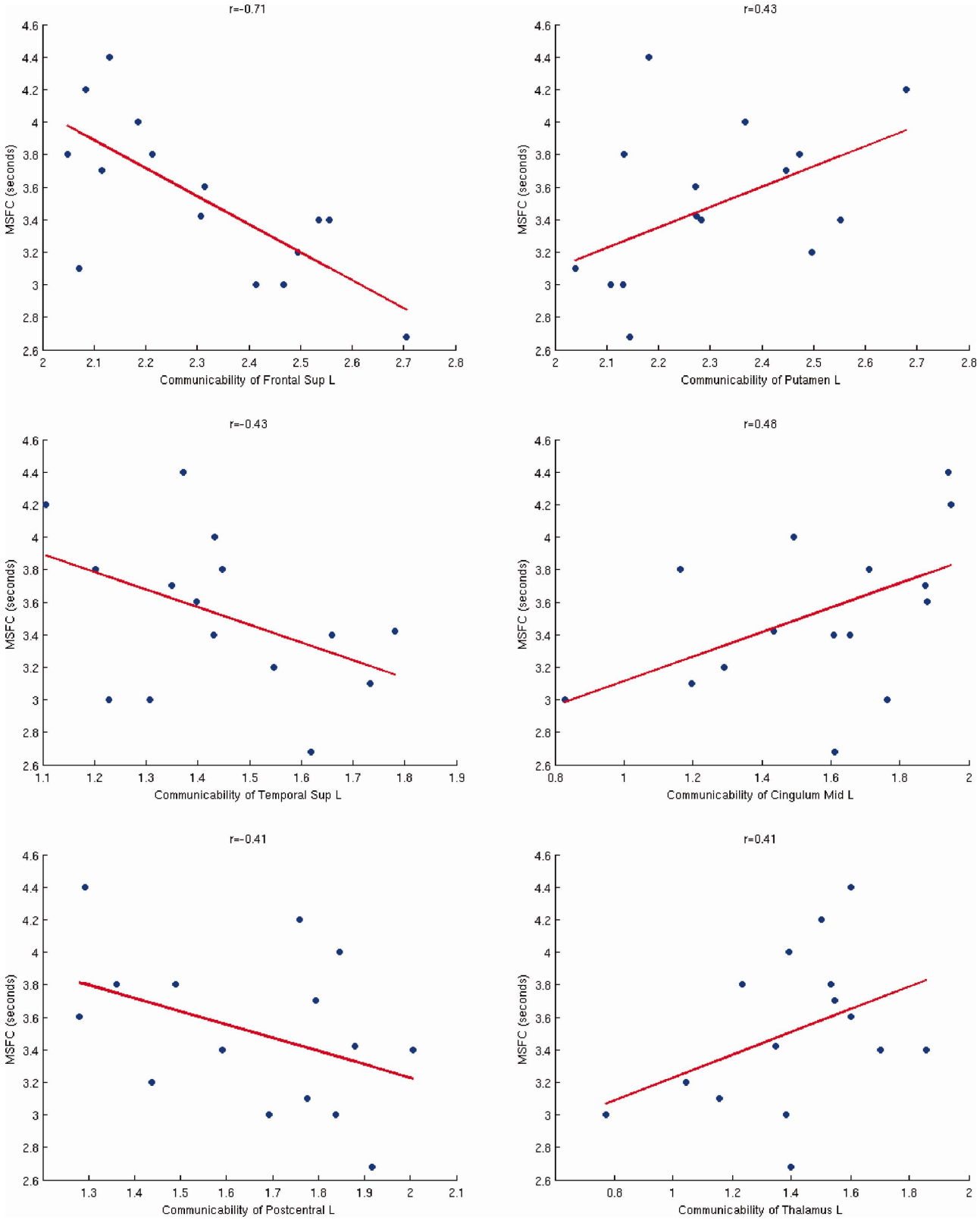

Figure 11.

The correlation between communicability and the MSFC Timed 25-foot Walk score. Left column: the regions with negative correlation. Right column: the regions with positive correlations. Note that only 15 (of 24) RRMS patients have the score for the Timed 25-foot Walk test. [Color figure can be viewed in the online issue, which is available at wileyonlinelibrary.com.]

TABLE III. Functions of the regions where statistically significant communicability changes were observed

Regions of neuroconnectivity changes	Function of region
L Precentral gyrus	Primary motor strip
L Rolandic opercular region	Word finding
L Pericentral lobule	Lower extremity sensory
L Hippocampus	Episodic memory
L Inferior occipital lobe	Vision
L Precuneus	Memory, visiospatial, consciousness
L Inferior temporal lobe	Written word processing
L Herschl gyrus	Pitch
L Putamen	Movement regulation
R Calcarine	Primary visual cortex
R Postcentral gyrus	Primary sensory cortex
R Inferior parietal region	Emotion, facial stimulus perception
R Parahippocampal region	Memory encoding
R Inferior opercular frontal lobe	On-line syntax building
R Superior occipital lobe	Vision
R Middle occipital lobe	Vision
R Posterior cingulum	Planning, attention
R Amygdala	Fear conditioning/anxiety

reorganization is likely to have several different substrates, including synaptic changes, increased recruitment of parallel existing pathways or "latent" connections, and reorganization of different sites [Filippi and Agosta, 2009]. Brain plasticity may play a major role in limiting the functional consequences of axonal injury and loss in MS [Filippi and Agosta, 2009], but only sequential neuroconnectivity DTI studies will test this hypothesis for validity, and determine if these changes have any predictive value.

Our study displayed significant decreases in neuroconnectivity and abnormal DTI indices within the OR of the RRMS group as depicted by areas of neuroconnectivity reductions in the occipital lobes as well as high-density lesions on the probability maps in the region of the optic tracts. When first examined, 30–50% of patients with MS manifest frank visual dysfunction [McDonald and Barnes, 1992; Reich et al., 2009]. In our MS cohort, nine of 24 patients were diagnosed with optic neuritis at some time point during this study. Significant reductions in neuroconnectivity in the RRMS group is in agreement with previous research using diffusion tensor magnetic resonance (DT-MR) tractography in MS patients with optic neuritis showing decreased connectivity values in both left and right OR when compared with controls [Ciccarelli et al., 2005]. These findings suggest the occurrence of trans-synaptic degeneration secondary to optic nerve damage and loss of afferent neurons in the lateral geniculate nucleus (LGN) [Evangelou et al., 2001]. Thus, reductions in neuroconnectivity may reflect a decrease in axonal density and volume within the OR fiber bundle, originating in the LGN [Ciccarelli et al., 2005]. Additionally, because the OR passes through the periventricular and subcortical white matter, the tract may be affected by focal demyelinating lesions that typically accumulate in these areas [Reich et al., 2009] as can be seen on our lesion probability map (Fig. 8). Furthermore, studies using fMRI have demonstrated a reorganization of the cerebral response to visual stimuli following optic neuritis recovery and have suggested that neural reorganization may represent an adaptive response to abnormal input [Werring et al., 2000; Toosy et al., 2002]. Hence, it is conceivable that at least part of this functional reorganization is associated with alterations in structural connectivity that participate in the transmission of visual stimuli [Ciccarelli et al., 2005].

Other unexpected findings in this study included significant loss of neuroconnectivity to the hippocampus and temporal lobes that would be expected to result in memory deficits. Other authors have also identified significant hippocampal disease using inversion recovery imaging [Roosendaal et al., 2008] as well as atrophy analysis, and revealed an associated correlation with deficits in memory encoding and retrieval [Sicotte et al., 2008]. It must be noted the functions of the hippocampal and frontal regions are not routinely assessed during clinic visits, although these deficits are known to be a major component of disability in MS, and could be assessed with neuropsychological testing for comparison in a controlled study.

LIMITATIONS

Limitations of the present study include its retrospective nature and selected minor issues with the neuroimaging protocol. DTI data was acquired in only six directions, although imaging parameters were considered optimal at the time of initial patient intake. This limited the ability of depicting the fibers with bifurcations/crossings. The posterior fossa and caudal brainstem were not assessed to reduce imaging time, increase patient comfort, and protect against artifact secondary to patient movement. The validity of this study is dependent on the accuracy of the AAL template. Recently, studies have demonstrated that network measures are sensitive to the number of ROIs (nodes in the network) and accuracy of its partitioning [Zalesky et al., 2010b]. Another limitation of the study is that the cognitive assessment was not performed prospectively as cognitive deficits were not thought to be a major component of the disease in this patient group who was gainfully used. Therefore, cognitive testing was not performed, but would be for any controlled future study if at all feasible, and would likely be addressed with the PASAT-3 of the MSFC. Despite these limitations, we are able to demonstrate statistically significant reductions of neuroconnectivity in our early RRMS patients, compared to NC using the new network analysis method, which is capable of dealing with indirect connections. Although MS is a very heterogeneous disease with a broad spectrum of disease expression and progression, we still believe that this information

needs to be made public to others who are interested in this area of research particularly as this technique appears to be a sensitive method for disease detection. This is a pilot study, and longitudinal studies in a larger patient cohort will be needed to further assess this technique, and to determine if measurable changes occur over time. Assessment of neuroconnectivity analysis in the frontal and temporal regions with comparison to neuropsychiatric testing may also substantiate our findings.

CONCLUSIONS

In conclusion, the present study using DTI-based neuroconnectivity analysis demonstrated quantifiable, structurally relevant alterations of fiber tract connections in a group of clinically early RRMS patients compared to NC, which confirms the work of previous authors, and expands upon their findings. Our results pave the way for longitudinal studies in larger patient groups, to elucidate both adaptive mechanisms contributing to limiting the clinical consequences of disease related tissue injury, and failure of such mechanisms results in the accumulation of irreversible disability. Partnering of sophisticated tools, such as neuroconnectivity analysis, with other MR imaging modalities expands the role of modern imaging applications related to MS. Future research in this area however is critical for understanding the underlying pathologic alterations and for development of therapeutic strategies for preventing propagation of neuronal dysfunction in MS.

REFERENCES

Aboitiz F, Scheibel AB, Fisher RS, Zaidel E (1992): Fiber composition of the human corpus callosum. Brain Res 598:143–153.

Ceccarelli A, Rocca MA, Valsasina P, Rodegher M, Falini A, Comi G, Filippi M (2010): Structural and functional magnetic resonance imaging correlates of motor network dysfunction in primary progressive multiple sclerosis. Eur J Neurosci 31: 1273–1280.

Charcot J (1868): Histologie de la sclerose en plaques, pp. 554–555. Gaz Hop Civils Militaires: Paris, France.

Ciccarelli O, Werring DJ, Wheeler-Kingshott CA, Barker GJ, Parker GJ, Thompson AJ, Miller DH (2001): Investigation of MS normal-appearing brain using diffusion tensor MRI with clinical correlations. Neurology 56:926–933.

Ciccarelli O, Toosy AT, Hickman SJ, Parker GJM, Wheeler-Kingshott CAM, Miller DH, Thompson AJ (2005): Optic radiation changes after optic neuritis detected by tractography-based group mapping. Hum Brain Mapp 25:308–316.

Compston A, Confavreux C, Lassmann H, McDonald I, Miller D, Noseworthy J, Smith K, Wekerle H (2006): McAlpine's Multiple Sclerosis. Elsevier: Amsterdam.

Crofts JJ, Higham DJ (2009): A weighted communicability measure applied to complex brain networks. J R Soc 6:411–414.

Crofts JJ, Higham DJ, Bosnell R, Jbabdi S, Matthews PM, Behrens TEJ, Johansen-Berg H (2010): Network analysis detects changes in the contralesional hemisphere following stroke. NeuroImage 54:161–169.

Estrada E, Hatano N (2008): Communicability in complex networks. Phys Rev E: Stat Nonlinear Soft Matter Phys 77:036111.

Evangelou N, Konz D, Esiri MM, Smith S, Palace J, Matthews PM (2001): Size-selective neuronal changes in the anterior optic pathways suggest a differential susceptibility to injury in multiple sclerosis. Brain 124:1813–1820.

Filippi M, Agosta F (2009): Magnetic resonance techniques to quantify tissue damage, tissue repair, and functional cortical reorganization in multiple sclerosis. Prog Brain Res 175: 465–482.

Filippi M, Iannucci G, Cercignani M, Assunta Rocca M, Pratesi A, Comi G (2000): A quantitative study of water diffusion in multiple sclerosis lesions and normal-appearing white matter using echo-planar imaging. Arch Neurol 57:1017–1021.

Filippi M, Rocca MA (2009): Functional MR imaging in multiple sclerosis. J Neuroimaging 19:59–70.

Goldberg II, Harel M, Malach R (2006): When the brain loses its self: Prefrontal inactivation during sensorimotor processing. Neuron 50:329–339.

Gong G, He Y, Concha L, Lebel C, Gross DW, Evans AC, Beaulieu C (2009): Mapping anatomical connectivity patterns of human cerebral cortex using in vivo diffusion tensor imaging tractography. Cerebral cortex. 19:524–536.

Guye M, Bettus G, Bartolomei F, Cozzone PJ (2010): Graph theoretical analysis of structural and functional connectivity MRI in normal and pathological brain networks. Magn Reson Mater Phys Biol Med 23:409–421.

Hasan KM, Gupta RK, Santos RM, Wolinsky JS, Narayana PA (2005): Diffusion tensor fractional anisotropy of the normal-appearing seven segments of the corpus callosum in healthy adults and relapsing-remitting multiple sclerosis patients. J Magn Reson Imaging 21:735–743.

Hasan KM, Halphen C, Kamali A, Nelson FM, Wolinsky JS, Narayana PA (2009): Caudate nuclei volume, diffusion tensor metrics, and T2 relaxation in healthy adults and relapsing-remitting multiple sclerosis patients: Implications for understanding gray matter degeneration. J Magn Reson Imaging 29:70–77.

He Y, Dagher A, Chen Z, Charil A, Zijdenbos A, Worsley K, Evans A (2009): Impaired small-world efficiency in structural cortical networks in multiple sclerosis associated with white matter lesion load. 132:3366–3379.

Lassmann H (2009): Axonal and neuronal pathology in multiple sclerosis: What have we learnt from animal models. Exp Neurol 225:2–8.

McDonald WI, Barnes D (1992): The ocular manifestations of multiple sclerosis. 1. Abnormalities of the afferent visual system. J Neurol Neurosurg Psychiatry 55:747–752.

Mottershead JP, Schmierer K, Clemence M, Thornton JS, Scaravilli F, Barker GJ, Tofts PS, Newcombe J, Cuzner ML, Ordidge RJ, McDonald WI, Miller DH (2003): High field MRI correlates of myelin content and axonal density in multiple sclerosis—A post-mortem study of the spinal cord. J Neurol 250:1293–1301.

Reich DS, Smith SA, Gordon-Lipkin EM, Ozturk A, Caffo BS, Balcer LJ, Calabresi PA (2009): Damage to the optic radiation in multiple sclerosis is associated with retinal injury and visual disability. Arch Neurol 66:998–1006.

Rocca MA, Colombo B, Falini A, Ghezzi A, Martinelli V, Scotti G, Comi G, Filippi M (2005): Cortical adaptation in patients with MS: A cross-sectional functional MRI study of disease phenotypes. Lancet Neurol 4:618–626.

Rocca MA, Agosta F, Martinelli V, Falini A, Comi G, Filippi M (2006): The level of spinal cord involvement influences the pattern of movement-associated cortical recruitment in patients with isolated myelitis. NeuroImage 30:879–884.

Rocca MA, Agosta F, Colombo B, Mezzapesa DM, Falini A, Comi G, Filippi M (2007): fMRI changes in relapsing-remitting multiple sclerosis patients complaining of fatigue after IFNbeta-1a injection. Hum Brain Mapp 28:373–382.

Roosendaal SD, Moraal B, Vrenken H, Castelijns JA, Pouwels PJW, Barkhof F, Geurts JJG (2008): In vivo MR imaging of hippocampal lesions in multiple sclerosis. J Magn Reson Imaging 27:726–731.

Rubinov M, Sporns O (2009): Complex network measures of brain connectivity: Uses and interpretations. NeuroImage 52:1059–1069.

Schmierer K, Wheeler-Kingshott CAM, Boulby PA, Scaravilli F, Altmann DR, Barker GJ, Tofts PS, Miller DH (2007): Diffusion tensor imaging of post mortem multiple sclerosis brain. NeuroImage 35:467–477.

Shu N, Liu Y, Li K, Duan Y, Wang J, Yu C, Dong H, Ye J, He Y (2011): Diffusion tensor tractography reveals disrupted topological efficiency in white matter structural networks in multiple sclerosis. Cereb Cortex 21:2565–2577.

Sicotte NL, Kern KC, Giesser BS, Arshanapalli A, Schultz A, Montag M, Wang H, Bookheimer SY (2008): Regional hippocampal atrophy in multiple sclerosis. Brain 131:1134–1141.

Skudlarski P, Jagannathan K, Calhoun VD, Hampson M, Skudlarska BA, Pearlson G (2008): Measuring brain connectivity: Diffusion tensor imaging validates resting state temporal correlations. NeuroImage 43:554–561.

Song S-K, Sun S-W, Ju W-K, Lin S-J, Cross AH, Neufeld AH (2003): Diffusion tensor imaging detects and differentiates axon and myelin degeneration in mouse optic nerve after retinal ischemia. NeuroImage 20:1714–1722.

Song S-K, Yoshino J, Le TQ, Lin S-J, Sun S-W, Cross AH, Armstrong RC (2005): Demyelination increases radial diffusivity in corpus callosum of mouse brain. NeuroImage 26:132–140.

Toosy AT, Werring DJ, Bullmore ET, Plant GT, Barker GJ, Miller DH, Thompson AJ (2002): Functional magnetic resonance imaging of the cortical response to photic stimulation in humans following optic neuritis recovery. Neurosci Lett 330: 255–259.

Tovar-Moll F, Evangelou IE, Chiu AW, Richert ND, Ostuni JL, Ohayon JM, Auh S, Ehrmantraut M, Talagala SL, McFarland HF, Bagnato F (2009): Thalamic involvement and its impact on clinical disability in patients with multiple sclerosis: A diffusion tensor imaging study at 3T. AJNR Am J Neuroradiol 30:1380–1386.

Trapp BD, Peterson J, Ransohoff RM, Rudick R, Mörk S, Bö L (1998): Axonal transection in the lesions of multiple sclerosis. N Engl J Med 338:278–285.

Tzourio-Mazoyer N, Landeau B, Papathanassiou D, Crivello F, Etard O, Delcroix N, Mazoyer B, Joliot M (2002): Automated anatomical labeling of activations in SPM using a macroscopic anatomical parcellation of the MNI MRI single subject brain. NeuroImage 15:273–289.

Verstraete E, Veldink JH, Mandl RCW, van den Berg LH, van den Heuvel MP (2011): Impaired structural motor connectome in amyotrophic lateral sclerosis. PloS one 6:e24239.

Wegner C et al. (2008): Relating functional changes during hand movement to clinical parameters in patients with multiple sclerosis in a multi-centre fMRI study. Eur J Neurol 15: 113–122.

Werring DJ, Bullmore ET, Toosy AT, Miller DH, Barker GJ, MacManus DG, Brammer MJ, Giampietro VP, Brusa A, Brex PA, Moseley IF, Plant GT, McDonald WI, Thompson AJ (2000): Recovery from optic neuritis is associated with a change in the distribution of cerebral response to visual stimulation: A functional magnetic resonance imaging study. J Neurol Neurosurg Psychiatry 68:441–449.

Wu G, Qi F, Shen D (2006): Learning-Based Deformable Registration of MR Brain Images. IEEE Trans. Medical Imaging, 25:1145–1157.

Yap P-T, Wu G, Zhu H, Lin W, Shen D (2010): F-TIMER: Fast tensor image morphing for elastic registration. IEEE Trans Med Imaging 29:1192–1203.

Zalesky A, Fornito A, Bullmore ET (2010a): Network-based statistic: Identifying differences in brain networks. NeuroImage 53:1197–1207.

Zalesky A, Fornito A, Harding IH, Cocchi L, Yücel M, Pantelis C, Bullmore ET (2010b): Whole-brain anatomical networks: Does the choice of nodes matter? NeuroImage 50:970–983.

Zhang D, Wang Y, Zhou L, Yuan H, Shen D (2011): Multimodal Classification of Alzheimer's Disease and Mild Cognitive Impairment. Neuroimage 55:856–867.

Zhang J, Wang J, Wu Q, Kuang W, Huang X, He Y, Gong Q (2011): Disrupted brain connectivity networks in drug-naive, first-episode major depressive disorder. Biol Psychiatry 70: 334–342.

APPENDIX

COMMUNICABILITY IN UNWEIGHTED GRAPHS

The "communicability" is first defined in an unweighted graph. Suppose that we are given a network, that is, a list of N nodes (such as N brain regions), along with a corresponding list of undirected edges connecting these nodes. Mathematically, this is an undirected, unweighted graph that can be defined in terms of an $N \times N$ adjacency matrix A whose ijth element is

$$a_{ij} = \begin{cases} 1 & \text{if there is an edge connecting nodes i and j} \\ 0 & \text{otherwise} \end{cases} \quad (1)$$

We always set a_{ii} 0, so that the self-links are not allowed.

Given the adjacency matrix of a graph, the degree of node i, that is, the number of edges incident to it, is given by

$$\deg_i = \sum_j a_{ij} \quad (2)$$

A useful observation is that the ijth entry of the kth power of the adjacency matrix

$$(A^k)_{ij} := \sum_{r_1=1}^{N} \sum_{r_2=1}^{N} \cdots \sum_{r_{k-1}=1}^{N} a_{i,r_1} a_{r_1,r_2} a_{r_2,r_3} \cdots a_{r_{k-2},r_{k-1}} a_{r_{k-1},j} \quad (3)$$

counts the number of walks of length k starting at node i and ending at node j. Here, a walk of length k is any traversal through the network that travels k edges. To let the longer walks have less influence than the shorter walks, $(A^k)_{ij}$ (walks of length k) is scaled by a factor of $1/k!$. This scaling is particularly important in our context because information–transformation noise is expected to increase with the walk length [Crofts et al., 2010]. In this way, communicability between two distinct nodes i and j are defined as

$$(A)_{ij} + \frac{(A^2)_{ij}}{2!} + \frac{(A^3)_{ij}}{3!} + \cdots \tag{4}$$

and can be written as $(\exp(A))_{ij}$, where exp denotes the matrix exponential. In other words, the communicability is a weighted sum of the number of walks between two nodes i and j, in which the bigger weightings of the shorter walks result in a larger contribution.

NETWORK COMMUNICABILITY IN WEIGHTED GRAPH

In our study, connectivity information, provided by the tractography step, takes the form of real-valued, positive weights. A larger weight a_{ij} indicates a greater 'strength' of connection between nodes i and j (Note that strength simply refers to the number of tractography streamlines that connect two nodes, or alternatively, the average FA or MD along a path). In this more general setting, both Eqs. (2) and (3) remain valid. However, their interpretation changes slightly. In Eq. (2), the notion of degree is replaced by the concept of a weighted or generalized degree. Therefore, rather than counting the number of edges incident to node i, we compute the sum of weights along incident edges. In the case of Eq. (3), rather than simply making a zero/one contribution depending on whether the walk $i \to r_1 \to r_2 \to \cdots \to r_{k-2} \to r_{k-1} \to j$ is possible, the term $a_{i,r_1}\, a_{r_1,r2} \cdots a_{r_{k-2},\, rk-1}\, a_{r_{k-1},j}$ represents the product of the weights along all the edges in the walk. Similarly, the degree of this weighted-network is defined as:

$$\deg_i = \sum_j a_{ij}$$

Although it is possible to define communicability for a weighted network as in Eq. (4), the difficulty is likely to arise if the weights are poorly calibrated. For example, nodes with unusually large weights often dominate the results. Thus, Crofts and Higham [2009] proposed a normalization step in which the weight a_{ij} is divided by the product $\sqrt{\deg_i \cdot \deg_j}$, such that communicability between distinct nodes i and j in a weighted network is defined as:

$$C_{ij} = (\exp(D^{-\frac{1}{2}} A D^{-\frac{1}{2}}))_{ij} \tag{5}$$

where $D^{-1/2} := \mathrm{diag}(1/\sqrt{\deg_i})$ is an $N \times N$ diagonal matrix. The study by Crofts and Higham [2009] showed that this new measure adds significant stability to the raw connectivity measures.

Note that the communicability matrix can in fact be used to define a new network C_{ij}, the so-called communicability network whose nodes coincide with those of the original network, but whose weighted links are given by Eq. (5). Therefore, other than C_{ij} that specifically indicates the communicability between nodes i and j, the degree of each node in C_{ij} gives a measure of the overall communicability between each node and all the other nodes in the network

$$\deg_{C_i} = \sum_j C_{ij} \tag{6}$$

Average Path Length

As reorganization of tracts may occur between the regions affected by the lesion, the reduced direct communicability may be compensated via connections with longer paths. Therefore, it is possible that in some situations, the overall communicability could be maintained. In this case, this kind of network change is invisible to the communicability metric proposed in the study by Crofts and Higham [2009]. To quantify this important information, we proposed a new network measurement, average path length (APL). Owing to the fact that a direct/shorter path is more efficient in information transmission, APL is not simply computed as the APL of a number of different pathways. Instead, using a similar idea, it is weighted by $k!$. In other words, APL is defined to measure the average length the information travels along different paths, when sending a unit amount of information between two nodes:

$$APL_{ij} = \frac{\frac{(A'^1)_{ij}}{1!} \cdot 1 + \frac{(A'^2)_{ij}}{2!} \cdot 2 + \frac{(A'^3)_{ij}}{3!} \cdot 3 + \cdots}{\frac{(A'^1)_{ij}}{1!} + \frac{(A'^2)_{ij}}{2!} + \frac{(A'^3)_{ij}}{3!} + \cdots} \tag{7}$$

where $A' = D^{-\frac{1}{2}} A D^{-\frac{1}{2}}$ is the normalized adjacency matrix. Therefore, Eq. (7) can be simplified further:

$$APL_{ij} = \frac{\sum_{k=1}^{\infty} \frac{(A'^k)_{ij}}{(k-1)!}}{\exp(A')_{ij}} \tag{8}$$